ZERO-G EXPERIMENTS OF THE BIONICWINGSAT - A 2U-CUBESAT WITH DEPLOYABLE, BIOLOGICALLY-INSPIRED WINGS

Martin E. Zander [(1)], Matthew K. Chamberlain [(2)], Dominic Jost [(1)] , Daniel Müller [(1)] , Marco Straubel [(1)]

[(1)] Institute of Lightweight Systems, DLR Deutsches Zentrum für Luft- und Raumfahrt e.V. (German Aerospace Center), 39108 Braunschweig, Germany,
Email: Martin.Zander@dlr.de
[(2)] NASA Langley Research Center, Hampton VA 23681, United States of America,
Email: matthew.k.chamberlain@nasa.gov

KEYWORDS

Deployable structures, Gossamer, biological inspired, zero-g, experiments, space

ABSTRACT

In this paper, recent testing of a novel deployable structure with several potential applications in space will be described, with the focus on performed deployment experiments in a DLR Zero-g flight campaign and in ground tests. Through a cooperative effort of the German Aerospace Center (DLR) and the National Aeronautics and Space Administration (NASA), a biologically-inspired structurally-integrated membrane featuring distributed functional elements has been developed and integrated into the 2U CubeSat called BionicWingSat. Such a membrane structure could be useful for all sorts of applications in which a relatively flat area is desirable such as solar sails, drag sails, or solar shades. For SmallSats and CubeSats, the design proposed also has the desirable property of being self-deploying without the need for powered deployment mechanisms. Building on previous work inspired by the wings of earwigs, the research presented in this paper focuses on testing of developed design concepts for such structural systems. To do so 24 fully integrated wings on two BionicWingSats in 2U Cubesat format were experimentally deployed in a microgravity environment during a dedicated DLR Zero-g flight campaign in 2021. The results of these experiments, the built hardware and test articles, the test arrangement, as well as a comparison to ground tests are discussed in this paper.

1. INTRODUCTION

Membrane dominated structures are generally used in space two purposes: to collect, reflect, and transmit electromagnetic radiation or for drag augmentation. Respective examples of such structures include reflectors and sun shields [1], solar sails [2-5], deorbiting sails [6,7] and solar arrays [8-9]. The high cost of launch vehicles and limited space inside launch vehicle shrouds dictate that such structures are generally designed to be lightweight and pack efficiently for launch while still being able to safely and consistently expand in space to achieve the desired geometry. Deployment and maintenance of the desired shape requires stiff structures and mechanisms to motivate the deployment and keep the structure flat, driving up the weight and complexity of the overall system. A simple means of deploying and structurally supporting membrane structures would thus be advantageous, particularly for SmallSat missions which face extreme mass and volume limitations. A biologically inspired hierarchical structure that can be deployed in space is proposed in this paper. This structure is meant to provide power using photovoltaic arrays for future SmallSats and CubeSats or other functional areas like solar shades, drag sails or solar sails, or even in low gravity environments as present on Earth´s moon.

In previous work, an integrated approach to develop a thin-film damage tolerant membrane incorporating a distributed support structure was explored using additive layer manufacturing (ALM). [11] A bio-inspired hierarchical structure was printed on films using additive layer manufacturing to achieve improved tear resistance, areal stiffness and to facilitate membrane deployment. Test results showed this initial work produced higher tear resistance than neat film of equivalent mass. [12,13] One application of particular interest previously was in power generation. If high packing efficiencies can be achieved using this integrated structural membrane approach, then larger photovoltaic (PV) arrays can be stowed in smaller spacecraft. Possible future applications for such deployable structural membrane systems are the PV arrays needed for solar electric propulsion (SEP) for beyond Earth orbit, large PV arrays on very small commercial spacecraft like Cubesats and Smallsats or even large PV arrays on crewed spacecraft such as the Orion crew capsule.

The work presented in this paper was carried out by the German Space Agency (DLR) and National Aeronautics and Space Administration (NASA) based on a vision for expanding the usefulness of the simple self-deploying biologically inspired membrane developed previously. While the focus in previous work was on power generation, such a light, large membrane structures can also be used for drag sails, solar shades, reflectors or other functional areas. Drag sails have gained greater

importance in the field of CubeSats with the introduction of a new United States Federal Communications Commission (FCC) rule requiring that all satellites in low earth orbit be deorbited within five years after the end of a mission [15]. For this reason, the new advanced self-deploying membrane structure tested was designed to be incorporated into a 2U CubeSat form factor for testing in a microgravity environment as if it were a functional drag sail. This paper specifically discusses microgravity deployment testing of the BionicWingSat structures whereas the development, detailed design, manufacturing and mechanical characterization of the wings are described in a previous publication [15].

2. DESIGN

2.1. Wing Design

Abstracting from previous work on earwigs [16, 17], several common hinge geometries were identified and designed in computer-aided design software (CAD) to create new elastic hinges that provide the folding and self-deploying function. ALM techniques allowed rapid iteration so that multiple generations could be designed, manufactured, and tested. In this way, it was discovered that some hinge geometries intended for one purpose might serve well in other roles based on the materials and design parameters selected. For instance, some hinges were abstracted from places in earwig wings where they provided out-of-plane bending but when manufactured out of thinner material capable of taking more strain, they provided good deployment torque when subjected to in-plane bending or twist. By changing material properties as the prototypes were created, a search for appropriate materials to make these hinges was conducted in parallel with the design effort. This design process is described in more detail in [15].

Originally, the drag sail wings were meant to be hierarchically ordered using various hinges idealized and optimized from earwig wings. Eventually, this idea was simplified to the structure as presented in Figure 1 a) and a simplified folding scheme. The wings are divided evenly into sections of a circle comprising 35 degrees of an arc. Each section has one, two or three lines of hinges with smaller hinges closer to the hub at the center of the spacecraft. Each section is bordered by radial stiffeners. In this way, the wing can be fan-folded at radial locations where the hinges line up. The fan-folded wings, as shown fixed in a central hub-interface in Figure 1 b), can then be wrapped around the central hub of the spacecraft, illustrated in Figure 1 c). The radial stiffeners wrapped around the hub provide the initial kick from their stored strain energy to begin deployment while the circumferentially arranged lines of oval hinges provide final motivation to spread the wing and stiffen it when deployed. The final size of the wing and its sections was determined based on the ability to store two wings and the central hub within the 1U (10 x 10 x 10 cm) space allotted to them in the BionicWingSat.

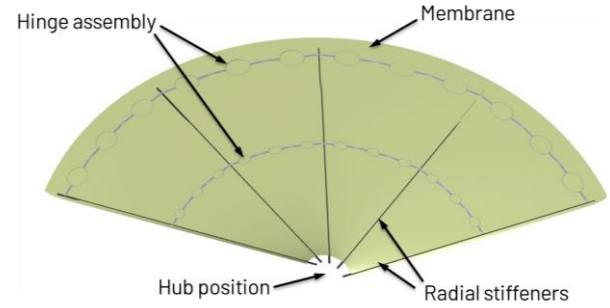

a) Main features

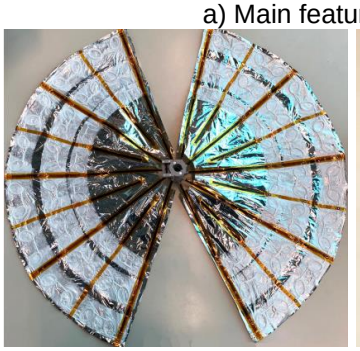

b) Deployed wings assembled on a hub (wing module)

c) Stowed wing

Figure 1: Main features of the wings of the BionicWingSat.

2.2. BionicWingSat Design

One of the key design constraints was the restriction of the packaged wing volume to a 1U space in a CubeSat. For this reason and to demonstrate future applicability to SmallSats, the microgravity experiment was designed resembling a 2U CubeSat with 1U volume reserved for wing storage and a second 1U volume dedicated to electronics, data acquisition, and mechanisms. The electronics and mechanism compartment contains the electronics board, a battery pack, a motor, and the mechanism to release the door. During a wing deployment, the stored wings are released two seconds after the four doors are unlocked and open. The motion of the door is rapid but damped by an adjustable hinge mechanism so that it takes two seconds to complete. To protect equipment and personnel during experiments the aluminum BionicWingSat main structure is covered with elastic safety bumpers at all sharp edges. The BionicWingSat in stowed configuration is depicted in the upper image of Figure 2. The wing compartment contains the two wings and the central hub (wing module). Once released, the two wings self-deploy outward in a symmetric circular fashion, reaching a nearly circular overall shape approximately 940 mm in diameter, as depicted in the lower image of Figure 2. Once the wings have been deployed in an

experiment, the wings and its hub can be quickly removed and replaced by a packed wing hub with two stowed and fixed wings. The additively manufactured hub connects each radial vein of a wing to the connecting each vein of a wing to the BionicWingSat (see Figure 1 c). Equipped with a leash for safety purposes, the BionicWingSat was retracted by the operator in the free-floating area during microgravity testing, thus preventing the BionicWingSat from dropping or crashing to the floor at the end of each 0-g phase. After each test run, the wing-hub-package was replaced, and the doors were manually closed and locked with onboard switches. The process of refurbishment - including unmounting deployed wings and mounting new packed wings on a hub- takes less than one minute and was performed during the 0-g phase of dedicated parabolas. The BionicWingSat is also equipped with an electronic board enabling a wireless control of all functions and hosting a gyroscope sensor, an accelerometer, and light emitting diodes (LEDs) to indicate the status of the systems onboard. It also includes several switches for manual control e.g., locking, unlocking and turning the power on or off. In addition to the onboard sensors, two small, rugged cameras were mounted on a BionicWingSat for visual documentation of the experiments.

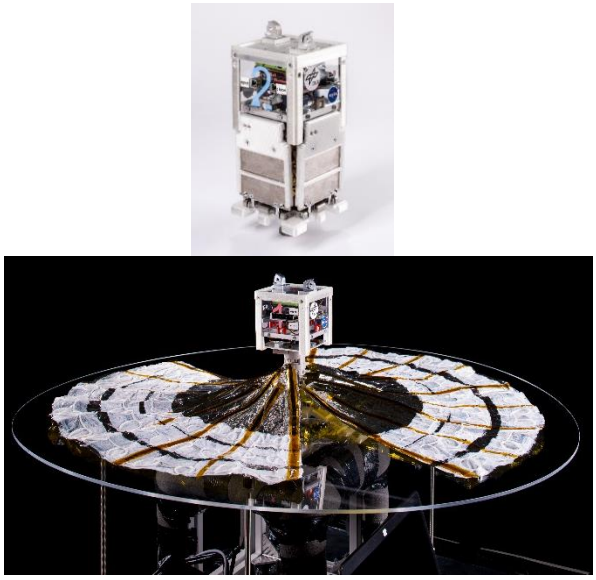

Figure 2: BionicWingSat stowed (upper), deployed in ground test rack (lower).

3. EXPERIMENTS

3.1. Principle and Methodology

3.1.1. Test setup

The BionicWingSat experiments were planned and set up to be tested in two configurations: a rack-bound configuration in which the BionicWingSat is fixed via quick mount to the test rack (see Figure 3 a); and the free-floating configuration in which the BionicWingSat is freely floating in a dedicated area (see Figure 3 b). In both configurations the BionicWingSat is remotely controlled from a laptop in the test rack, commanding system activation, door opening and wing release. Moreover, measured sensor data and housekeeping data are fed back live via Bluetooth to the data acquisition system (DAQ) into LabView.

Experiments in the rack-bound configuration started with a BionicWingSat mounted to the rack, with closed and locked doors, holding the stowed wings inside. When the carrier aircraft reached a steady microgravity level the BionicWingSat was remotely triggered to open its doors and then release its wings as illustrated in Figure 3 a). During deployment, the laptop in combination with a DAQ system acquired sensor data from rack integrated sensors as well as from sensors onboard the BionicWingSat.

In the free-floating configuration deployment experiments were carried out in a dedicated area enclosed by a net. The BionicWingSat was held by an operator and placed in the middle of the area once a steady microgravity was achieved and released to float freely, while the doors were still closed. Door opening and wing deployment were then initiated as illustrated in Figure 3 b).

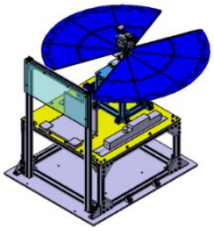

a) Rack-bound configuration – deployed.

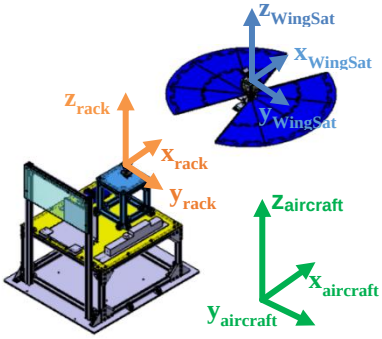

b) Free-floating configuration – deployed.

Figure 3: Test configurations and aligned test coordinate systems: BionicWingSat (blue), rack (orange), aircraft (green).

The overall layout of the aircraft cabin, with the test rack and free-floating area displayed, is illustrated in Figure 4 a). To carry out the planned twelve deployment experiments in the two configurations with twelve different samples, a storage box was used and placed close to the rack for easy access (see Figure 4 a). The box contained all prepared samples (stowed wings on exchangeable hubs) prior to use as well as the wing sets that had been

deployed already, both BionicWingSats, and some tools. To safely perform all tasks of the experiment including refurbishment, three operators were necessary. The first operator was operating the rack and DAQ system, the second was responsible for refurbishment near the storage box, while the third was operating the BionicWingSats in the free-floating area. In addition to the two cameras mounted on a BionicWingSat, three cameras mounted on rails of the aircraft cabin were used to monitor the deployment experiments from a third person view (see Figure 4 a). Examples of the rack-bound and free-floating experiments performed during 0-g phase are shown in the images (b) and (c) of Figure 4, respectively.

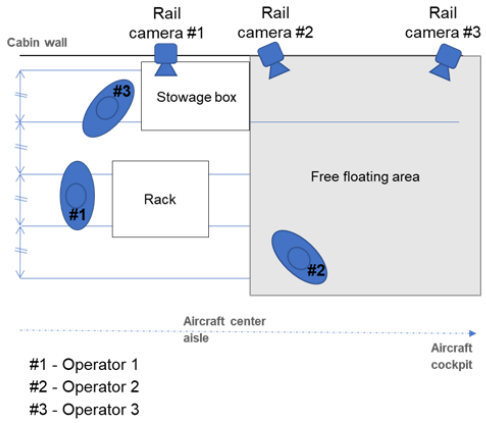

a) Test setup in airplane

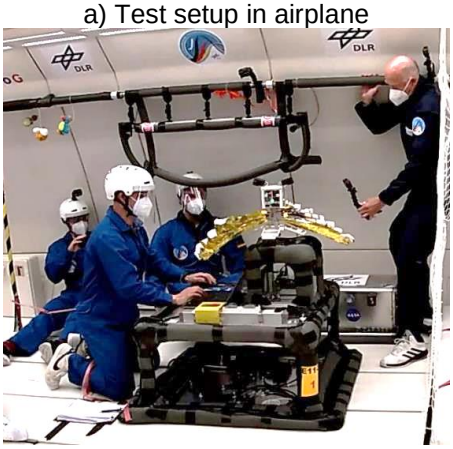

b) Testing in rack-bound configuration.

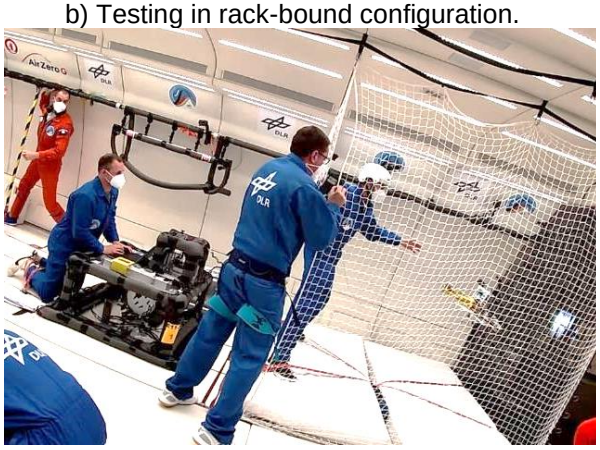

c) Testing in free-floating configuration.

Figure 4: Test configurations during in-flight testing (0-g phase).

3.1.2. Test procedure

The rack-bound experiments were performed within the first eleven parabolas. The parabolas in between were used for refurbishment of the BionicWingSat and for re-equipping it with a new, still stowed, wing module (hub with stowed wings). The tested and deployed wings including its hub were stowed away as soon as they are removed from the BionicWingSat. In the scheduled breaks within the overall flight refurbishment, an exchange of camera batteries and back-stowing of the deployed wing modules was performed. After finishing the last experiment in parabola #23, all samples, BionicWingSats and tools were stowed away in the stowage box.

3.2. Results

The results of each of the twelve microgravity experiments are described in this subsection. For each parabola and sample onboard sensor data of BionicWingSat and rack were analyzed along with the video footage taken. Each of the test configurations provided different sets of useful data. The rack-bound configuration delivered results for the door opening dynamics and forces, while the free-floating configuration primarily provided results on door opening signals, wing deployment and the associated dynamic responses of the satellite.

In general, the quality of the microgravity environment produced by the aircraft parabolic maneuver was good. Microgravity with < ±0.03 g in all axes was provided for about 20 s out of each parabola. The accelerometer data from the aircraft provided the achieved microgravity level. However, a residual gravity, while small, was enough to cause the BionicWingSat to drift when released in the free-floating area, occasionally resulting in it impacting the net enclosure and ending the deployment experiment. More physical interactions between the BionicWingSat, rack and aircraft were visible in the rack-bound configuration. A dynamic excitation about all axes of the mounted BionicWingSat was observed during these parabolas, caused by the aircraft engines, transmitted thru the floor rails into the fixed rack. This excitation is reflected in the results discussed in the following paragraphs, as vibration amplitudes exceed amplitudes e.g. of wing deployment, making some of the sensor data unusable.

3.2.1. Rack-bound Experiments

The rack-bound configuration was the first to be tested. All six wing types were deployed each in separate parabolas. Although all test runs are started and ended in the 0-g phase, strong vibrations were induced by the airplane during testing as well as some data loss of the DAQ system occurred. Thus, only two of six test runs generated analyzable sensor data output. Nevertheless, all test runs delivered video footage of deployment

behavior. The most valuable results from the rack-bound tests are the forces measured at the base of the fixed BionicWingSat, especially the forces measured in the z-axis of the BionicWingSat. In , the graphs of the two analyzable test runs are showing the exerted force in z-axis F_z over time. In order to relate the loads measured with the state of the door opening and wing release, the angle of the servo motor of the hold down release mechanism (HDRM) is shown. The steps of the unlock and release sequence are marked with numbers one through six, as shown in the top portion of Figure 5.

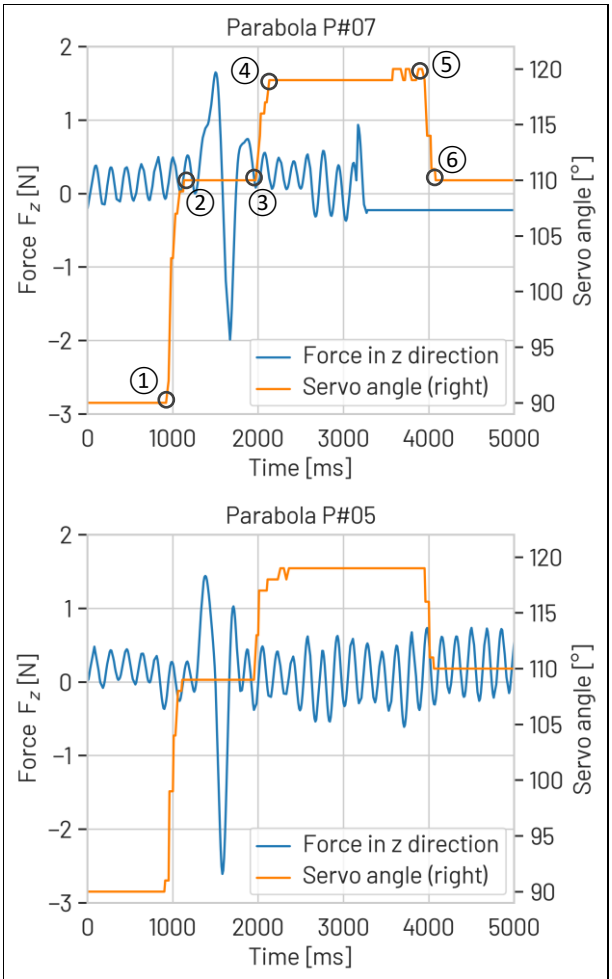

Unlock and release sequence (upper left image):
① doors opening initiated (unlocking)
② doors unlocked
③ wings release initiated
④ wings released
⑤ HDRM set back (to handling state) initiated
⑥ HDRM in handling state

Figure 5: Forces in z-axis exerted by the BionicWingSat doors during rack-bound deployment tests.

Starting the test run with the BionicWingSat mounted to the rack, the doors were locked and the packaged wings were tightly held in place. Even in this phase, the airplane vibrations are visible in the graph as well as in the video footage. The sequence started at mark ① with the doors opening, initiated by turning the release mechanism from 90° to about 0°. At mark ② the door unlocking process was completed and the doors began to swing open. The swinging is visible in the rising F_z amplitude in upwards (positive) direction, as the lowering doors were pushing the BionicWingSat upwards. The decrease of amplitude marks the doors reaching their end stop with a smaller subsequent bounce backward.

In Table 1, the detected maxima and minima forces with F_{zMax} and F_{zMin} are provided along with the time at event and the corresponding servo angle. Here the first peaks (F_{zMax}) are between 1.4 N and 1.7 N, while the second peaks (F_{zMax}) are between -2.6 N and 2.0 N. The force exerted is thus repeatable. After about two seconds, the wing release was initiated (at mark ③ in) by increasing the servo angle, δ, to 117°. At mark ④ the wings were released starting their self-deployment. The release event however is not noticeable in the force amplitude as the vibrations overlay the very small forces exerted by the wings. Nevertheless, only very small forces in z-direction were expected due to the radial wing deployment.

Table 1: Maximum and minimum forces in z-axis of the rack-mounted BionicWingSat

Para-bola	*Wing sample type*	t_{FzMax} *[ms]*	F_{zMax} *[N]*	δ_{FMax} *[°]*	t_{FzMin} *[ms]*	F_{zMin} *[N]*	δ_{FMin} *[°]*
P#05	D-I2-I3-I5-iv	1380	1.4	109	1580	-2.6	109
P#07	N-I2-I5-iv	1500	1.7	110	1670	-2.0	110

Each test run was ended when the HDRM was set back to the handling state starting at mark ⑤ and end at mark ⑥ at about 110° servo angle. In the handling state, the wing sample can be replaced with an undeployed one for the next test run, as described previously. The data gathered demonstrates that the door opening has an impact on the dynamics of the BionicWingSat itself and may be valuable in predicting induced motion for a satellite with similar wing systems.

3.2.2. Free-floating

In the free-floating configuration all six samples were successfully tested. The unlock and release sequence remained the same as performed during testing in rack-bound configuration. At the start of each test run, the BionicWingSat was released by the operator hovering in the free-floating area during the 0-g phase. While freely floating the doors were unlocked and open followed by the wing release about 2 s later. As soon as the wings were released the BionicWingSat started rotating about its z-axis deploying its wings. The complete deployment process is depicted in the sequence of images

shown in Figure 6. On several parabolas, the residual g-vectors during the 0-g phase led the BionicWingSat to drift into the net of the free-floating area before the wings were able to flatten out completely. When analyzing the onboard data of the gyroscope of the BionicWingSats, the rotating behavior also becomes apparent, as shown in the plots of the angular acceleration α_z of the BionicWingSat about its z-axis is plotted over time of Figure 7. As before, the angle of the servo motor of the release mechanism is plotted in order to identify the associated event of the unlock and release sequence. One can observe that the angular acceleration starts, with decreasing negative angular acceleration, about the BionicWingSat z-axis at mark ③, as soon as the wing release was initiated and the wings start to unfurl. The peak angular rotation (minimum), α_{zMin}, was reached in the middle of the self-deploying process of the wings at about three seconds. This behavior can be observed for all wing types and parabolas in the free-floating configuration. After a peak negative angular acceleration is an acceleration in the opposite direction until reaching an almost steady state with a quasi-constant angular velocity. This visible reduction of angular acceleration after achieving the handling state at mark ⑥ at about 110° servo angle can be attributed to the BionicWingSat drifting into the surrounding net, due to residual g-vectors, and to the retraction of the safety leash by the operator. In parabolas #2, #7, #21 and #23 an unfurling wing wiped across the rubberlike elastic safety bumpers of a satellite door and resulted in a rotation of the wing itself, that lead to a disturbed deployment and to possible further dynamics of the BionicWingSat.

The data for this test configuration is summarized in Table 2. The values for the angular acceleration at its peak at α_{zMin} are in the same range from -212.4 rad/s² to -272.4 rad/s² over all test wing types. Additionally, these peaks all occur at almost the same time, approximately 3000 ms after the normalized start of recording (normalized to 1000 ms before door opening is initiated at mark ①).

When comparing results within one wing sample type, the three samples of parabolas #12, #16 and #21 produce very similar values with a minimum angular acceleration α_{zMin} of -212.4 rad/s² ~ -240.8 rad/s² ~ -229.4 rad/s². The similarity in accelerations and the time of occurrence of the peak indicate a good repeatability as one can observe in Table 3. The two similar samples of parabola #15 and #17 with values for α_{zMin} of -272.4 rad/s² ~ -268.9 rad/s² also exhibited peak acceleration at the times.

Of the three different sample wing types, wing type D-I2-I5 produces the highest angular accelerations, followed by wing type N-I2-I5-iv and lastly wing type D-I2-I5-iv. Although the wing types N-I2-I5-iv and D-I2-I5-iv feature an identical design, the difference in angular acceleration can be attributed to the different build material of the hinge assemblies, thus generating different deployment forces and moments.

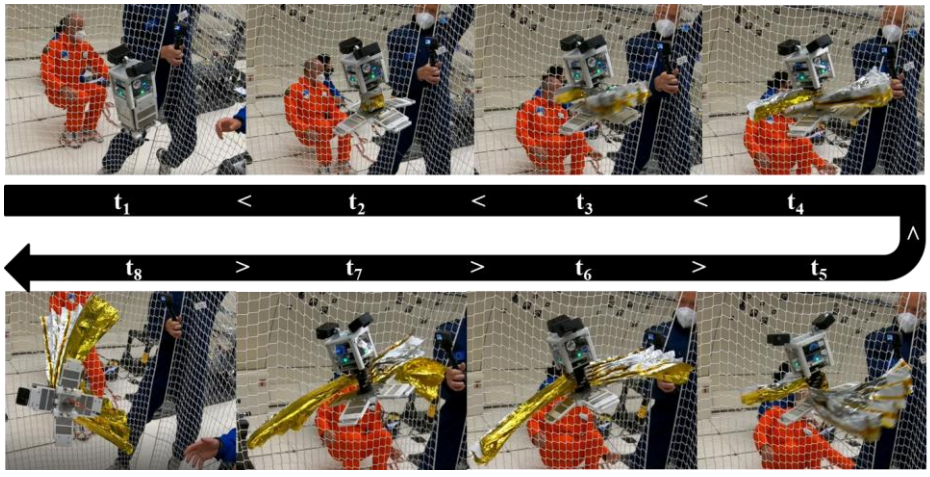

Figure 6: Time lapse of free-floating BionicWingSat.

Table 2: Minimum angular accelerations of free-floating BionicWingSat during wing deployment.

Parabola	*Wing sample type*	t_{Min} *[ms]*	α_{zMin} *[rad/s²]*	$\delta_{\alpha zMin}$ *[°]*
P#12	D-I2-I5-iv	2950	-212.4	117
P#15	D-I2-I5	3010	-272.4	119
P#16	D-I2-I5-iv	3080	-240.8	119
P#17	D-I2-I5	3020	-268.9	118
P#21	D-I2-I5-iv	2910	-229.4	119
P#23	N-I2-I5-iv	3340	-250.7	117

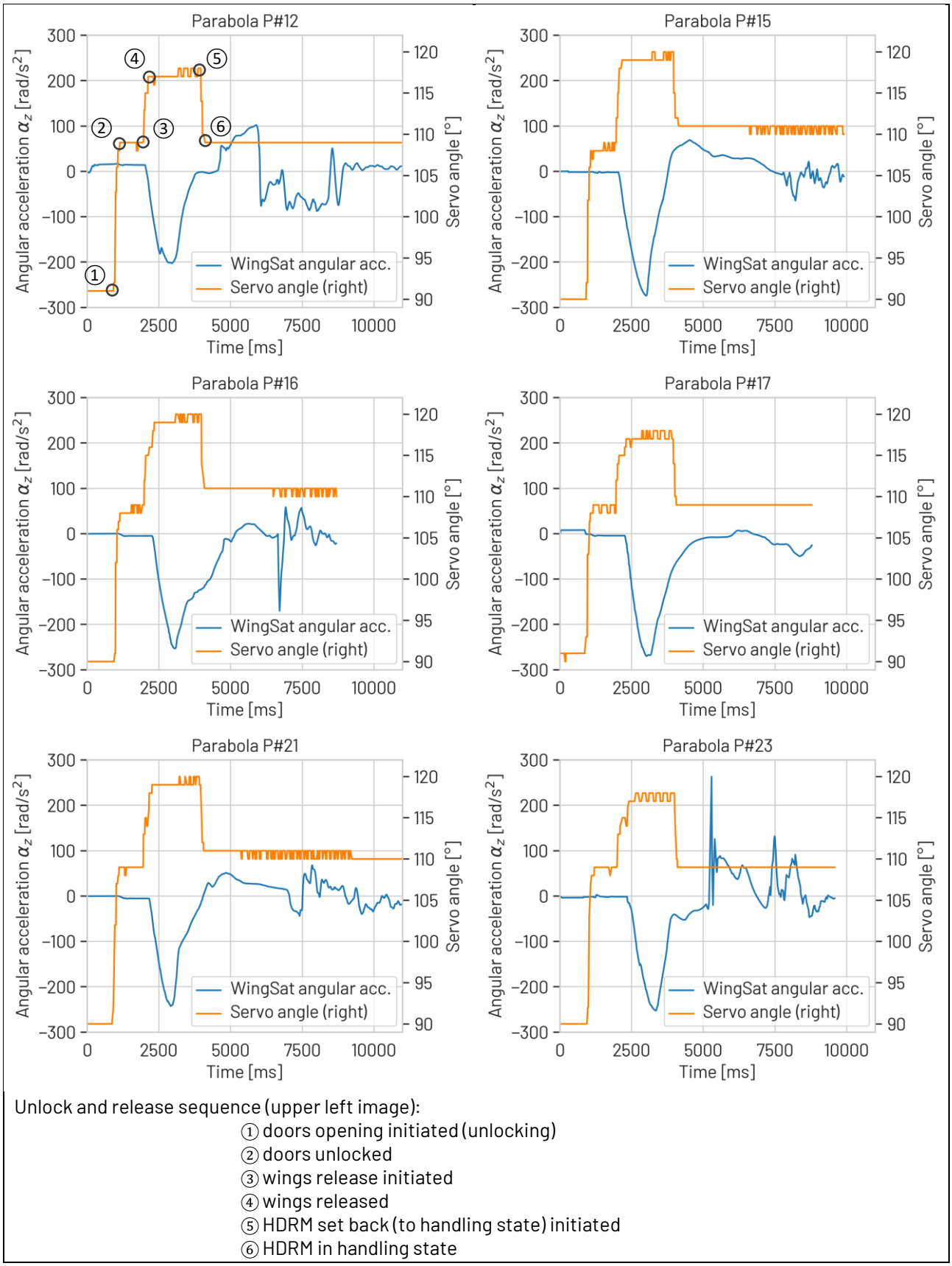

Unlock and release sequence (upper left image):

① doors opening initiated (unlocking)
② doors unlocked
③ wings release initiated
④ wings released
⑤ HDRM set back (to handling state) initiated
⑥ HDRM in handling state

Figure 7: Angular acceleration of BionicWingSat during free-floating deployment tests.

Moreover, a translational acceleration a_z of the BionicWingSat when freely floating is caused by the opening doors exerting an impulse by a flapping motion. This motion results in alternating accelerations, that are well visible in the exemplary graphs of parabolas #15 and #17, in Figure 8. Here the difference in the damping setup of the doors of the two BionicWingSats can also be observed when comparing the two graphs. While the amplitudes for parabola #15 is in a range between 1 and -0.5 m/s^2, flown on BionicWingSat #1, the amplitudes generated with BionicWingSat #2, in parabola #17, in a range between 2.5 m/s^2 and 0.7 m/s^2. Note that the amplitudes of a_z following the door opening are caused by the BionicWingSat floating into the surrounding net and by manually pulling back the satellite sample on its safety string the operator, as indicated in the upper graph of Figure 8. Thus, the acquired data may provide the basis for the prediction of dynamics of such a satellite, caused by the used door mechanism, in an actual flight case.

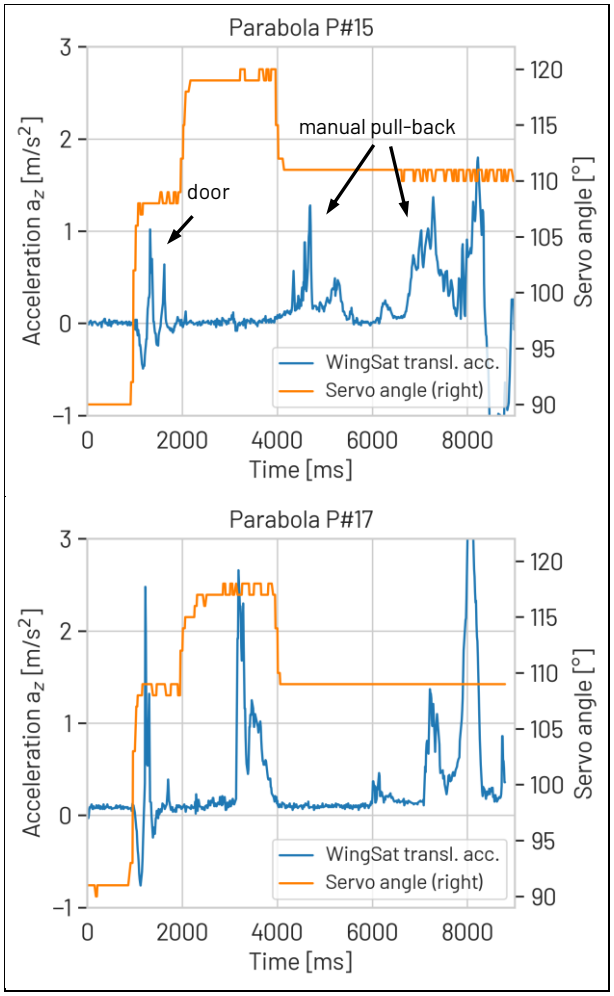

Figure 8: Translational acceleration along z-axis exerted by the BionicWingSat doors in free-floating test configuration.

Flatness

The cameras in the experiment had originally been intended for use in measuring the flatness of the deployed wings but proved not to be useful during the microgravity tests. Nevertheless, the video footage provided images, as presented in Figure 9, for a qualitative assessment of flatness and a simplified flatness estimation by image measuring. Residual accelerations induced motion throughout the free-flying tests however, and several samples ran into the safety nets, making it difficult to even give a qualitative assessment of which wing type was most flat at the point of full deployment. For all wings, creep in the hinge materials residual plastic deformations seemed to be the main driver for not achieving the original flatness they had during manufacturing, as one can observe for a rack-bound and a free-floating example in the images of Figure 9 a) and b) respectively. However, five samples from the rack bound configuration could be analyzed and flatness was measured using a software tool determining the ratio between the nominal and measured angle ε between two radial stiffeners, as illustrated in Figure 10. As a result a flatness between 48% to 60% was determined, with 100% resembling ideal flatness.

a) Parabola #2 – Rack bound deployment.

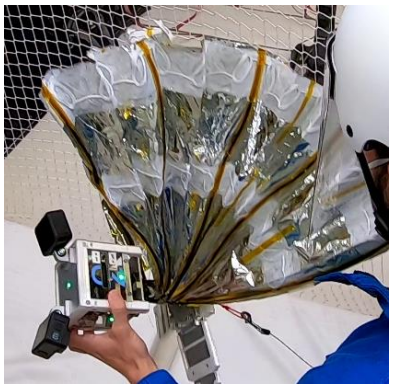

b) Parabola #15 – Free-floating deployment.

Figure 9: Flatness of deployed wings in rack-bound and free-floating configurations.

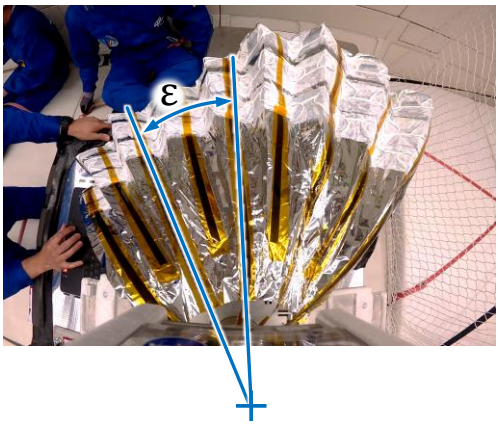

Figure 10: Flatness determined by image measurements of deployed wings.

3.2.3. Ground Testing

Prior to the microgravity experiments, ground tests similar to the rack-bound test configuration were performed. In order to simulate a 0-g environment, an attempt was made to compensate for gravity using a table that supports the deploying wings, while not hindering door opening. The adjustments made the test to reduce the coefficient of sliding friction between the deploying wings and the gravity compensation table are shown in Figure 11. After using the bare Plexiglas, the table was covered with paper, nylon fleece, and in one version the gravity table was omitted completely (see images of Figure 11). Consequently, the best results for deployment were achieved by covering the gravity compensation table with nylon fleece. Nevertheless, the influence of gravity was still apparent in deployment, creating effects not expected in a parabolic flight.

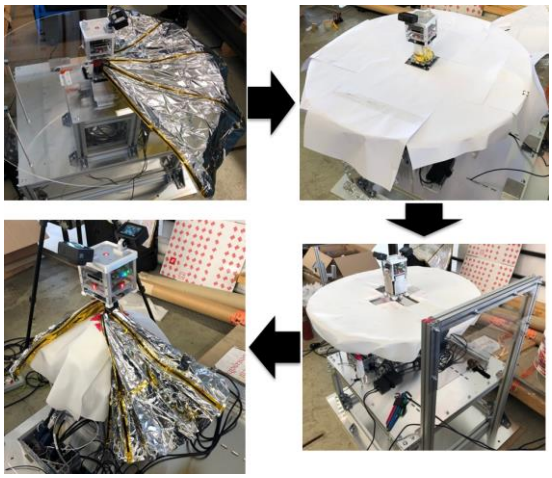

Figure 11: Ground test setup with variations of gravity compensations.

The test procedure is the same as done in the rack-bound configuration in the 0-g experiments. However, due to the increased friction between the unfolding wings and the gravity compensation, a manual deployment support, to deploy the wings flat, was necessary. The obtained measurements were mainly analyzed regarding the longitudinal force F_z exerted onto the BionicWingSat and the test rack by door opening and wing deployment. An exemplary graph of such results for one deployment is shown in Figure 12.

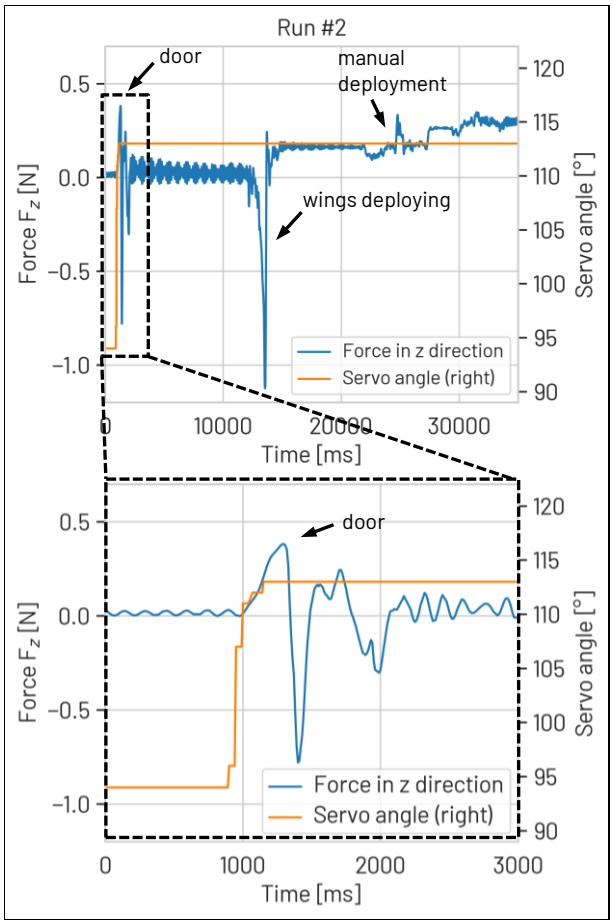

Figure 12: Forces in z-axis exerted by the BionicWingSat in ground deployment tests (lower image: augmented graph).

Here the current position of the servo and the force in z-direction (F_z) exerted by the BionicWingSat on the test stand during a ground test are shown over time. When observing the force curve, it can be divided into three events. The actuation of the servo changes its angular position and the doors of the CubeSat are opened before the wings are released and deployed. In the first event the force F_z is therefore generated by the door opening, with the doors bouncing in a flapping motion. With an augmented representation of this event, in the lower image of Figure 12 this effect is clearly visible in oscillating force amplitudes. This result coincides with the observations made for the rack-bound experiments for the 0-g experiments. However, the amplitudes itself are lower, although one would expect higher amplitudes due to gravity. Higher amplitudes can be explained be the necessity to adjust and lower the damping of the doors for a more rapid door opening in the 0-g experiments. Furthermore, some oscillations can be observed due to the sensitive force sensor and the design of

the satellite-rack-interface. Further force peaks are visible at the event of wing opening, when the wings deploy and partially fall onto the gravity compensation table, and when wing deployment is manually supported to achieve full flatness, as indicated in Figure 12.

Apart from delivering limited measurements, ground testing was used to improve the overall design. Testing of early designs revealed the need for increasing the opening forces of the elastic wing elements and for a size reduction of the wings for better integrability into the satellite. Nevertheless, in the performed ground tests it was not possible to determine mechanical differences of the wing design variations due to the friction effects between the test stand and the wings. It can be concluded that ground tests as performed only to provide basic information on the mechanical behavior and some measurements on the mechanism, since gravity has a significant influence.

4. CONCLUSION

In this paper, a design for a biologically inspired and structurally integrated drag sail membrane was tested in microgravity and on ground. Experiments in microgravity and on ground show that while the wing concept is functional, many aspects of the vison of self-deploying integrated structures still need to be improved. Microgravity testing showed that the hinge structures that were capable of self-deploying at a subscale on the ground were incapable of doing this in the short period of time available. It is possible that in space, such structures would finish deploying but in the parabolic flight where microgravity is immediately followed by a period of high gravity, this could not be shown. Further investigation into creep resistance is needed to solve this problem or else a more energetic structure capable of fully deploying in a short time period must be used.

During microgravity testing, several observations were made that were backed up by measured data. First, despite damping, the opening of the doors imparted measurable force on the rest of the satellite, meaning that in free flight it would induce motion. In free-flight, video and accelerometer data document that the deployment of the doors induced translational motion while the deployment of the wings consistently produced angular acceleration about the z-axis of the vehicle. Different types of wings were shown to produce different amounts of angular acceleration as they unfurled. That the highest acceleration values come from wing type D-I2-I5 generated came at a surprise, as the intermediate radial stiffener is thought to increase deployment forces and improve flatness. However, since additional elements on a wing are a trade-off between deployment forces by stored strain energy and additional fold lines coupled with an increase of friction when unfolding, the higher values for D-I2-I5 are assumed to have its origin in lower friction forces to be overcome when deploying. Moreover, some design features led to effects that were not observed in previous ground testing under gravity. For example, the safety bumpers introduced late in the design process may have caused the wings to rotate unintentionally and flip during the deployment process as the doors were apparently not moved out of the way to the necessary degree, thus disturbing a free deployment for some instance.

Testing in microgravity on a parabolic flight proved more challenging for this structure than expected. In the rack-mounted configuration, vibrations from the plane's engines were transmitted through the floor, exciting the BionicWingSat and saturating any acceleration measurements. Pre-flight analysis of the dynamics of the rack and CubeSat system might have identified this as a risk. In free flight, the tiny amounts of remaining acceleration in microgravity caused the BionicWingSat to coast into the netting walls, ruining some data and making it hard to judge wing flatness during several tests. A larger enclosure would have given the wings more time to deploy but with residual creep still present in the deployed structures, the parabolas still did not provide enough time to see if the wings would return to being flat in true microgravity. Knowing this, future tests should be limited to structures that deploy more quickly or which can be gravity offloaded between parabolas to allow continued deployment when microgravity returns. The prior ground deployment tests provided limited data, as the influence of gravity on such delicate structures is high. Nevertheless, it provided good information on necessary design iterations of the wings and the door mechanism as well as on the HDRM.

The work presented in this paper is envisioned as a step in a longer process of developing self-deploying membrane structure. Future research could choose to address these aspects individually, improving wing design for packing efficiency with material for space with low creep tendencies, looking for a manufacturing method that truly integrates the structure into the membrane without adhesive, and finding a way to reproduce these results with space-rated materials.

5. ACKNOWLEDGMENTS

This research has been carried out under an Implementing Arrangement between the NASA and the German Aerospace Center for Cooperative Research on Deployable Composite Booms.
The authors would like to thank DLR Space Research and Technology directorate and its former chair Prof. Dr. Hans-Jörg Dittus, the DLR institute director Professor Martin Wiedemann, as well as the head of DLR Department of Composite Design Prof. Dr. Christian Hühne for funding and supporting the microgravity test campaign. Moreover, the authors would like to acknowledge the support of

the NASA Space Technology Mission Directorate Game-Changing Development Deployable Composite Booms project, the NASA Langley Research Center, Structural Dynamics Branch, Dr. Martin Annett, and Dr. Keith Belvin, Dr. Olive Stohlman and Dr. Jin Ho Kang provided value advice on adhesion strategies. This work would not have been possible without the tireless efforts, ingenuity, and curiosity of NASA interns Ms. Amy Caldwell and Ms. Danielle DaCosta.

6. REFERENCES

1 Ewing, A.P., Back, J.M., Schuettpelz, B.M., and Laue, G.P., “James Webb Space Telescope Sunshield Membrane Assembly,” *50th AIAA/ASME/ASCE/AHS/ASC Structures, Structural Dynamics, and Materials Conference*, 4-7 may, 2009, Palm Springs, CA, AIAA 2009-2156

2 Mori O, Shirasawa Y, Mimasu Y et al., “Overview of IKAROS Mission: Part I Flight Programs,” Macdonald M (ed) *Advances in Solar Sailing*. Springer, pp. 25–43, 2014.

3 Spencer, D., Betts, B., Bellardo, J., Diaz, A., Plante, B., and Mansell, J., “The LightSail 2 Solar Sailing Technology Demonstration,” , Advances in Space Research (ASR), Vol. 67, Issue 9, pp. 2878-2889.

4 Johnson, L., Everett, J., McKenzie, D., Tyler, D., Wallace, D., Wilson, J., Newmark, J., Turse, D., Cannella, M., and Feldman, M., “The NASA Solar Cruiser Mission – Solar Sail Propulsion Enabling Heliophysics Missions,” *36th Annual Small Satellite Conference, Logan*, UT, 6-11 August, 2022, SSC22-II-03

5 Lockett, T.R., Castillo-Roger, J., Johsnon, L., Matus, J. Lightholder, J., Marinan, A., and Few, A., , "Near-Earth Asteroid Scout Flight Mission," in *IEEE Aerospace and Electronic Systems Magazine*, vol. 35, no. 3, pp. 20-29, 1 March 2020.

6 Stohlman, O., Fernandez, J.M., Lappas, V., Hillebrandt, M., Hühne, C., and Straubel, M., “Testing of the DeorbitSail Drag Sail Subsystem,” *54th AIAA/ASME/ASCE/AHS/ASC Structures, Structural Dynamics, and Materials Conference*, April 8-11, 2013, Boston, MA, AIAA 2013-1907

7 Alhorn, D.C., Casas, J.P., Agasid, E.F., Adams, C.L., Laue, G., Kitts, C., and S. O’Brien, “NanoSail-D: The Small Satellite That Could!”, 25th Annual AIAA/USU Conference on Small Satellites, Logan, August, 2011, UT, SSC11-VI-1.

8 Brady, T. K. and Sweeney, D. J., “International Space Station (ISS) Solar Array Wing (SAW) Lessons Learned, NASA TM-2011-217064, Vols. 1 & 2, March 2011.

9 Banik, J.A., and Hausgen, P., "Roll-Out Solar Arrays (ROSA): Next Generation Flexible Solar Array Technology for DoD Spacecraft," *2017 AIAA SPACE and Astronautics Forum and Exposition*, 12-14 September 2017, Orlando, Florida. AIAA-2017-5307.

10 Johnson, C. L., Carr, J., Fabisinski, L., Russell, T., and Smith, L., "Lightweight Integrated Solar Array (LISA): Providing Higher Power to Small Spacecraft," in *13th International Energy Conversion Engineering Conference, AIAA Propulsion and Energy Forum,* (AIAA 2015-3896), 2015.

11 Belvin, Zander et al., U.S. Provisional Patent Application for “Manufacturing of Low Mass, Large-Scale Hierarchical Thin Film Structural Systems,” No. 61/431,245, filed on January 10, 2011.

12 Belvin ,W. K., Zander, M. E., Sleight ,D. W., Connell, J., Holloway, N., and Palmierix, F., “Materials, Structures and Manufacturing: An Integrated Approach to Develop Expandable Structures,” in *53rd AIAA/ASME/ASCE/AHS/ASC Structures, Structural Dynamics, and Materials Conference*, Waikiki, Honolulu, Hawaii, 2012, AIAA 2012-1951.

13 Zander, M. E. and Belvin W. K., “Concept-Development of a Structure Supported membrane for Deployable Space Applications – From Nature to Manufacture and Testing,” in in *European Conference of Spacecraft Structures, Materials & Environmental Testing*, Noordwijk, The Netherlands, 2012.

14 Foust, J., “FCC to Set Five Year Deadline for Deorbiting LEO Satellites,” *Space News*, 8 Sept, 2022, https://spacenews.com/fcc-to-set-five-year-deadline-for-deorbiting-leo-satellites/, Accessed on 5 December, 2022.

15 Zander, M. E., Chamberlain, M. K., Jost, D., Müller, D., Hagmeister, N., Straubel, M., “Design and Testing of the BionicWingSat in a Zero-g Flight Campaign - A 2U-CubeSat with Deployable, Biologically-Inspired Wings,” AIAA SciTech 2023 Forum, 23–27 January 2023, National Harbor, MD & Online, AIAA 2023-1882.

16 Haas, F.; Gorb, S., and Wootton, R.J., “Elastic Joints in Dermapteran Hind Wings: Materials and Wing Folding,” in: *Arthropod Structure & Development*, Vol.29, p. 137-146, Elsevier Science Ltd., 2000.

17 Faber, J. A., Arrieta, A. F., and Studart, A. R., “Bioinspired Spring Origami”, *Science*. DOI: https://doi.org/10.1126/science.aap7753, 2018, p. 1386–1391.